INFRARED-EXCITED RED, GREEN, VIOLET AND UV LUMINESCENCE FROM LANGASITE CRYSTAL DOPED WITH ERBIUM AND YTTERBIUM

A. M. VOICULESCU, S. GEORGESCU, C. MATEI, A. G. STEFAN,
L. GHEORGHE, A. ACHIM, F. VOICU

National Institute for Laser, Plasma and Radiation Physics, 409 Atomistilor Street, Magurele, Ilfov, 077125, Romania, E-mail: ana.voiculescu@inflpr.ro

Received March 23, 2012

Red (665 nm), green (525 nm and 550 nm), violet (410 nm), and ultraviolet (380 nm) luminescence from a $La_{2.85}Yb_{0.12}Er_{0.03}Ga_5SiO_{14}$ (LGS) single crystal synthesized by the Czochralski technique was obtained by pumping at 973 nm. Yb^{3+} - Er^{3+} energy transfer processes accounting for the population of the emitting levels are discussed. The increase of temperature of the irradiated zone was estimated from the difference between the slopes of the of 525 and 550 luminescence intensity vs. pump intensity in a double logarithmic plot.

Key words: Upconversion, Luminescence, Langasite, Er^{3+}, Yb^{3+}

1. INTRODUCTION

The search of new fluorescent markers for applications in biology and medicine is a very actual problem. The phenomenon of upconversion represents the conversion of pump radiation in shorter-wavelength radiation, following the excitation of a quantum system by successive photon absorptions, energy transfer, or cooperative processes. These materials are applicable as upconversion pumped visible lasers [1, 2], displays [3, 4], biomarkers [5, 6] etc. The most investigated pair of dopants is Er^{3+}, as activator, and Yb^{3+} as sensitizer.

$La_3Ga_5SiO_{14}$ (LGS) belongs to a family of oxide compounds which form crystals having a $Ca_3Ga_2Ge_4O_{14}$ type structure [7]. The LGS crystals belong to the space group P321, class 32, and, accordingly, they are expected to exhibit piezoelectric and nonlinear optical properties. The langasite crystals have been investigated extensively in the past [8]. Recently, studies on crystal growth and properties of $La_3Ga_{5.5}Ta_{0.5}O_{14}$ (LGT) and $La_3Ga_{5.5}Nb_{0.5}O_{14}$ (LGN) revealed that these materials are promising for acousto-electronic applications and for the design of piezoelectric sensors [9, 10]. Advantageously important optical activity of LGT and LGN has been noticed, too.

Other promising features of all the crystals mentioned above is related to the fact that they can be doped by both rare earth and transition metal ions. Laser performance of LGS doped with neodymium has been investigated thoroughly [11].

Langasite, langatate and langanite are partially disordered crystals, *i.e.*, one of the crystallographic positions is shared by two different ions. This results in inhomogeneously broadened absorption and fluorescence lines. This was first considered an advantage for laser emission: wider absorption lines result in an efficient pumping while wider emission lines means tunability. For phosphors, the broadened absorption bands match better the emission of the pump laser diode.

The red luminescence of Eu^{3+} doped in LGS and LGT crystals was analyzed in [12-14]. The luminescence properties of Eu-doped LGN nanocrystals synthesized by a sol-gel method were discussed in [15]. Recently, we discussed the green and red upconversion luminescence in LGT doped with erbium and ytterbium synthesized by solid state reaction [16].

In this paper, we continue our investigations concerning the upconversion luminescence of the compounds from the langasite family, analyzing the upconversion luminescence in a LGS single crystal doped with erbium and ytterbium.

2. EXPERIMENTAL

The starting material, according to the formula $La_{2.85}Yb_{0.12}Er_{0.03}Ga_5SiO_{14}$, was prepared by the solid-state reaction of the 4N purity La_2O_3, Yb_2O_3, Er_2O_3, Ga_2O_3 and SiO_2. The oxide powders were weighed and mixed by milling in an agate mortar until a fine powder was obtained. After that, the obtained powder was cold-pressed into cylindrical pellet and reacted by heating at 1350°C for 36 h.

$La_{2.85}Yb_{0.12}Er_{0.03}Ga_5SiO_{14}$ single crystal (starting composition) was grown by the Czochralski technique, along c-axis, in an iridium crucible (30 mm - diameter, 30 mm – height) in N_2 atmosphere using a pure LGS seed. In order to avoid the formation of polycrystals in the growth process, preheating at a temperature 50-60°C higher than the melting point was required. Then, the temperature was reduced to the growth temperature. The pulling rate was 1 mm/h and the rotation rate was about 25 rpm. The growth temperature, determined by an infrared pyrometer, was about 1470 ± 10°C. The temperature gradient just above the melt was 30 - 40°C/cm. As much as 20% of the melt was converted into a single crystal in approximately three days. The crystal was cooled to room temperature at a rate of 40°C/h. In order to eliminate the residual stress inside the crystal, it was annealed further in air atmosphere. The crystal was heated to 1350°C at the rate of 50°C/h, held at this temperature for 36h, and finally slowly cooled to room temperature at the rate of 20°C/h.

The luminescence of LGS:Er:Yb was excited in IR, at 973 nm, using the laser diode JOLD-150-CANN-3A. The experimental set-up for luminescence measurements contains a Horiba Jobin-Yvon monochromator (model 1000MP), a

S-20 photomultiplier and the SR 830 lockin amplifier on line with a computer. All the measurements were performed at room temperature.

3. RESULTS AND DISCUSSION

The upconversion luminescence spectra for pumping at 973 nm are given in Figs. 1 and 2. In Fig. 1, are shown the green ($^2H_{11/2} \rightarrow {}^4I_{15/2}$ and $^4S_{3/2} \rightarrow {}^4I_{15/2}$) and red ($^4F_{9/2} \rightarrow {}^4I_{15/2}$) luminescence bands. In Fig. 2, the luminescence bands corresponding to $^4G_{11/2} \rightarrow {}^4I_{15/2}$ (at ~ 380 nm, in near UV) and $^2H_{9/2} \rightarrow {}^4I_{15/2}$ (at ~ 410 nm, violet) transitions are observed.

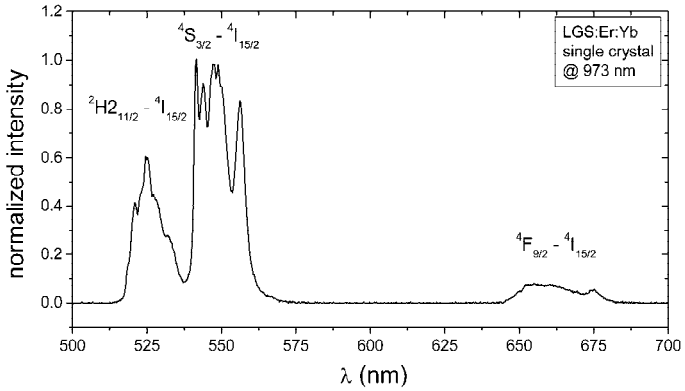

Fig. 1 – Upconversion pumped (at 973 nm) luminescence spectrum of LGS:Er:Yb single crystal. The green (transitions $^2H_{11/2} \rightarrow {}^4I_{15/2}$ and $^4S_{3/2} \rightarrow {}^4I_{15/2}$) and red luminescence ($^4F_{9/2} \rightarrow {}^4I_{15/2}$) is observed. The spectrum is not corrected for the spectral responsivity of the experimental apparatus.

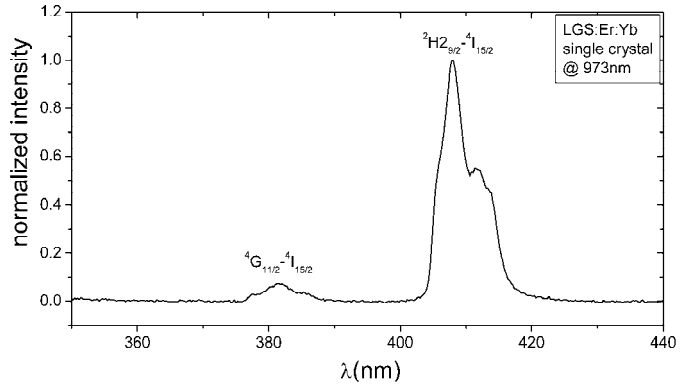

Fig. 2 – Upconversion pumped UV ($^4G_{11/2} \rightarrow {}^4I_{15/2}$) and violet ($^2H_{9/2} \rightarrow {}^4I_{15/2}$) luminescence of LGS:Er:Yb single crystal. The spectrum is not corrected for the spectral responsivity of the experimental apparatus.

The double logarithmic plot of the green ($^2H_{11/2} \rightarrow {}^4I_{15/2}$ - at ~ 525 nm and $^4S_{3/2} \rightarrow {}^4I_{15/2}$ - at ~ 550 nm), red ($^4F_{9/2} \rightarrow {}^4I_{15/2}$, ~ 665 nm) and violet ($^2H_{9/2} \rightarrow {}^4I_{15/2}$, 410 nm) luminescence integral intensity, function of the incident IR pump power, is given in Fig. 3. The slopes of these dependences are 1.85 and 1.76 (green luminescence), 1.68 (red luminescence) and 2.66 (violet luminescence). The intensity of the $^4G_{11/2} \rightarrow {}^4I_{15/2}$ luminescence was too low to allow a reliable measurement of its pump power dependence.

For low pump intensities, the intensity (I_l) of the upconverted luminescence depends on the pump intensity (P) according to the relation [17]:

$$I_l \propto P^n \tag{1}$$

where n is the number of photons necessary to reach the emitting level.

The values of the slopes in the double logarithmic plot in Fig. 3 indicate two-photon processes for green and red luminescence and a three-photon one for the violet luminescence.

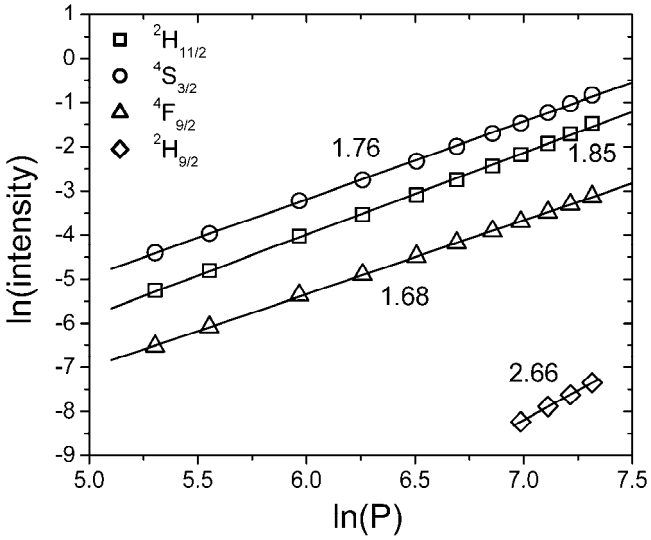

Fig. 3 – Double logarithmic plot of green ($^2H_{11/2} \rightarrow {}^4I_{15/2}$ – squares, $^4S_{3/2} \rightarrow {}^4I_{15/2}$ - circles), red ($^4F_{9/2} \rightarrow {}^4I_{15/2}$ - triangles) and violet ($^2H_{9/2} \rightarrow {}^4I_{15/2}$ - diamond) luminescence intensity function of the incident IR powder. The slopes of these dependences are shown.

At room temperature, the Er^{3+} levels $^2H_{11/2}$ and $^4S_{3/2}$ are thermalized and the ratio between their integral luminescence intensities depends on temperature. Therefore, if the temperature remains unchanged, they should exhibit the same slope n in the double logarithmic plot (Fig. 3). The observed difference (Δn) can be explained by the temperature increase of the irradiated zone of the sample for increasing pump power [16]. The ratio of the areas of the luminescence bands in

the luminescence spectrum is proportional with the ratio of the radiative transition probabilities multiplied with ratio of their populations [18, 19]. Assuming that the ratio of the radiative transition probabilities does not change, the ratio between the areas of $^2H_{11/2} \rightarrow {}^4I_{15/2}$ and $^4S_{3/2} \rightarrow {}^4I_{15/2}$ luminescence depends only of the ratio of their populations, which is temperature dependent.

It can be shown that the variation of temperature Δt, when the pump power increases from P_1 to P_2, can be expressed by the approximate relation [20]

$$\Delta t \approx \frac{k_B T_1^2}{\Delta E} \Delta n \ln\left(P_2 / P_1\right) \approx 77 \Delta n \ln\left(P_2 / P_1\right) \tag{2}$$

where T_1 (= 300K) is the initial temperature of the sample corresponding to the (weak) pump power P_1, $\Delta E \approx 800$ cm^{-1} is the energy gap between $^2H_{11/2}$ and $^4S_{3/2}$ in the two-level approximation and k_B is the Boltzmann constant. In Fig. 3, $\Delta n = 0.09$. For $\ln(P_2/P_1)=2$ (the incident power excursion in the experiment depicted in Fig. 3); it results $\Delta t \approx 14$ºC.

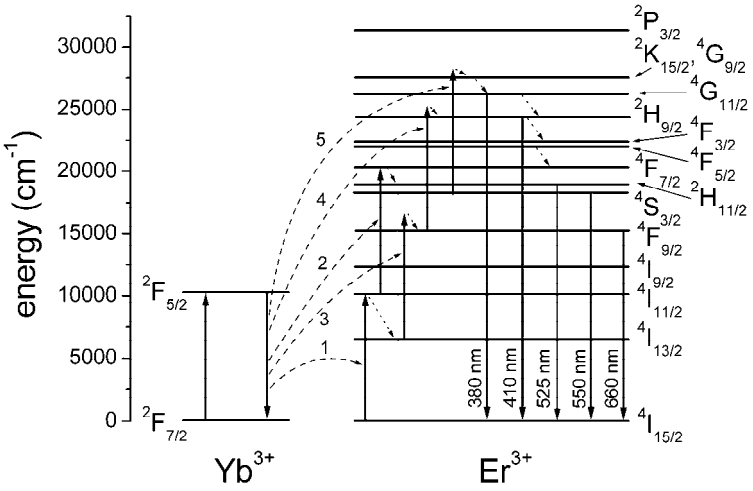

Fig. 4 – Energy level diagram of Yb^{3+} and Er^{3+} in LGS and proposed upconversion mechanisms. The energy transfer processes between Yb^{3+} and Er^{3+} are indicated by curved dashed arrows. Dotted arrows show multiphonon transitions. The average wavelengths of the observed luminescent transitions are also given.

In order to explain the observed upconversion luminescence, we propose the following $Yb^{3+} \rightarrow Er^{3+}$ energy transfer processes (see Fig. 4):

(1) $^2F_{5/2}$ (Yb^{3+}) + $^4I_{15/2}$ (Er^{3+}) → $^2F_{7/2}$ (Yb^{3+}) + $^4I_{11/2}$ (Er^{3+});

(2) $^2F_{5/2}$ (Yb^{3+}) + $^4I_{11/2}$ (Er^{3+}) → $^2F_{7/2}$ (Yb^{3+}) + $^4F_{7/2}$ (Er^{3+}) $\xrightarrow{multiphonon}$ ($^2H_{11/2}$, $^4S_{3/2}$) (Er^{3+});

(3) $^2F_{5/2}$ (Yb^{3+}) + $^4I_{13/2}$ (Er^{3+}) $\rightarrow$ $^2F_{7/2}$ (Yb^{3+}) + $^4F_{9/2}$ (Er^{3+}) + phonons;

(4) $^2F_{5/2}$ (Yb^{3+}) + $^4F_{9/2}$ (Er^{3+}) $\rightarrow$ $^2F_{7/2}$ (Yb^{3+}) + $^2H_{9/2}$ (Er^{3+}) + phonons;

(5) $^2F_{5/2}$ (Yb^{3+}) + $^4S_{3/2}$ (Er^{3+}) $\rightarrow$ $^2F_{7/2}$ (Yb^{3+}) + $^2K_{15/2}$, $^4G_{9/2}$ (Er^{3+}) $\xrightarrow{multiphonon}$ $^4G_{11/2}$ (Er^{3+}).

The $^2H_{11/2}$, $^4S_{3/2}$ levels of Er^{3+} are populated, mainly, by the processes (1) and (2); a small contribution comes from the higher Er^{3+} levels, by multiphonon transitions. The $^4F_{9/2}$ (Er^{3+}) level is populated by processes (1) and (3) and by the multiphonon transition from $^2H_{11/2}$ and $^4S_{3/2}$. For $^2H_{11/2}$, $^4S_{3/2}$ and $^4F_{9/2}$, the main contribution is given by two-photon processes, as reflected in the values of the slopes in the ln-ln plot in Fig. (3).

The $^2H_{9/2}$ (Er^{3+}) level is populated by a three-photon process since this level is situated at an energy (~ 24400 cm^{-1}) which is more than two times the energy of the pumping laser (~ 10280 cm^{-1}); one more photon is necessary to reach the $^2H_{9/2}$ (Er^{3+}) level starting either from Er^{3+} levels $^2H_{11/2}$, $^4S_{3/2}$ or from $^4F_{9/2}$. Since the difference between the slopes of $^2H_{9/2}$ (Er^{3+}) and $^4F_{9/2}$ (Er^{3+}) in the double logarithmic plot in Fig. 3 is approximately 1, we consider the process (4) the main process responsible for the population of the $^2H_{9/2}$ (Er^{3+}) level.

As we discussed before, for low pump levels, the luminescence intensity satisfy the Eq. (1) [17]. The slopes of the green and red luminescence in Fig. 3 are less than 2, being 1.85, 1.76, and 1.68, respectively. This can be explained by the saturation of the intermediary Er^{3+} levels ($^4I_{13/2}$, $^4I_{11/2}$) involved in the population of the emitting levels. A detailed discussion concerning the saturation effects can be found in [21].

4. CONCLUSIONS

The langasite single crystal doped with erbium and codoped with ytterbium was grown in nitrogen, using the Czochralski technique. Green, red, violet, and UV luminescence was obtained for pumping at 973 nm. Five $Yb^{3+} \rightarrow Er^{3+}$ energy transfer processes were proposed in order to explain the observed upconversion luminescence. We found that the Er^{3+} level $^2H_{9/2}$, responsible for the violet luminescence, is fed, mainly, from the $^4F_{9/2}$ level. As the result of the irradiation with 973 nm photons, the temperature of the irradiated zone increases slightly, as expressed by the slope difference Δn between the green luminescence bands in the double logarithmic plot. We found that Δn is very sensitive to the temperature increase of the sample.

Acknowledgments. This work was supported by the Romanian National Research Council (CNCS) in the frame of the Projects PD 51/05.10.2011 and IDEI 82/06.10.2011.

REFERENCES

1. O. Hellmig, S. Salewski, A. Stark, J. Schwenke, P. E. Toschek, K. Sengstock, V. M. Baev, Opt. Lett. **35**, 2263–2265 (2010).
2. E. Osiac, E. Heumann, G. Huber, S. Kück, E. Sani, A. Toncelli, M. Tonelli, Appl. Phys. Lett. **82**, 3832–3834 (2003).
3. Z. M. Yang, Z. M. Feng, Z. H. Jiang, J. Phys. D **38**, 1629–1632 (2005).
4. Q. H. Wang, M. Bass, Electron. Lett. **40**, 987–989 (2004).
5. M. Wang, C. C. Mi, W. X. Wang, C. H. Liu, Y. F. Wu, Z. R. Xu, C. B. Mao, Sh. K. Xu, ACS Nano **3**, 1580–1586 (2009).
6. K. Kuningas, T. Rantanen, T. Ukonaho, T. Lovgren, T. Soukka, Anal. Chem. **77**, 7348–7355 (2005).
7. E. L. Belokoneva, A. V. Butashin, M. A. Simonov, B. V. Mill, N. V. Belov, Dokl. Akad. Nauk. SSR, **255**, 1094–1097 (1980).
8. A. A. Kaminskii, B. V. Mill, G. G. Khodzhabagyan, A. F. Konstantinova, A. I. Okorochkov, I. M. Silvestrova, Phys. Status Solidi (a), **80**, 387–398 (1983).
9. J. Bohm, R. B. Heimann, M. Hengst, R. Roewer, J. Schindler, J. Cryst. Growth, **204**, 128–136 (1999).
10. J. Bohm, E. Chilla, C. Flannery, H. J. Froechlich, T. Hauke, R. B. Heimann, M. Hengst, U. Straube, J. Cryst. Growth, **216**, 293–298 (2000).
11. A. A. Kaminskii, I. M. Silvestrova, S. E. Sarkisov, and G. A. Denisenko, Phys. Status Solidi (a), **80**, 607–620 (1983).
12. S. Georgescu, O. Toma, L. Gheorghe, A. Achim, A. M. Chinie, A. Stefan, Optical Materials **30**, 212–215 (2007).
13. S. Georgescu, O. Toma, A. M. Chinie, L. Gheorghe, A. Achim, A. S. Stefan, Optical Materials **30**, 1007–1012 (2008).
14. S. Georgescu, O. Toma, A. M. Chinie, L. Gheorghe, A. Achim, A. S. Stefan, J. Lumin. **128**, 741–743 (2008).
15. S. Georgescu, A. M. Voiculescu, O. Toma, S. Nastase, C. Matei, M. Osiac, J. Alloys Compnd. **507**, 470–474 (2010).
16. S. Georgescu, O. Toma, A. M. Voiculescu, C. Matei, R. Birjega, L. Petrescu, Physica B, **407**, 1124–1127 (2012).
17. M. Pollnau, D. R. Gamelin, S. R. Lüthi, H. U. Güdel, Phys. Rev. B **61**, 3337–3346 (2000).
18. S. F. Collins, G. W. Baxter, S. A. Wade, T. Sun, K. T. V. Grattan, Z. Y. Zhang, A. W. Palmer, J. Appl. Phys. **84**, 4649–4654 (1998).
19. S. A. Wade, S. F. Collins, G. W. Baxter, J. Appl. Phys. **94**, 4743–4756 (2003).
20. S. Georgescu et al., will be published.
21. G. Chen, G. Somesfalean, Y. Liu, Z. Zhang, Q. Sun, F. Wang, Phys. Rev. B **75**, 195204 (2007).